

Decoding the QCD critical behaviour in A + A collisions[☆]

N. G. Antoniou^{a,*}, N. Davis^b, F. K. Diakonos^a, G. Doultinos^a, N. Kalntis^a,
 A. Kanargias^a, A. S. Kapoyannis^a, V. Ozvenchuk^b, C. N. Papanicolas^{a,c},
 A. Rybicki^b, E. Stiliaris^a

^a*Faculty of Physics, University of Athens, GR-15784 Athens, Greece*

^b*Institute of Nuclear Physics, Polish Academy of Sciences, Kraków, Poland*

^c*The Cyprus Institute, Nicosia, Cyprus*

Abstract

In a systematic search for the QCD critical point in nuclear collisions, at the CERN SPS, it was found that intermittency measurements in the freeze-out state of central Si + Si collisions, at the maximum SPS energy, provide us with an indication of sizeable critical fluctuations. Also, rather recently, a weaker effect was traced in preliminary data of the Ar + Sc reaction for 10 – 20% most central collisions at (approximately) the same energy. However, the uncertainties in the analysis and the limitations of the experimental event statistics make the interpretation of the above measurements (NA49, NA61/SHINE) rather inconclusive, inviting for a further, phenomenological investigation with complementary tools and theoretical ideas. To this end, in the present work, we employ intermittency techniques within a model-independent analysis scheme (AMIAS), a novel method from Data Science [1], in order to produce unbiased results for the parameters of the power-laws and in particular for the associated power-law exponent (intermittency

[☆]Dedicated to the memory of N. G. Antoniou (1939-2020)

*deceased

Email addresses: nantonio@phys.uoa.gr (N. G. Antoniou), Nikolaos.Davis@ifj.edu.pl (N. Davis), fdiakono@phys.uoa.gr (F. K. Diakonos), georgedoultinos@gmail.com (G. Doultinos), nikos.kalntis@gmail.com (N. Kalntis), akanaryias@hotmail.com (A. Kanargias), akapog@phys.uoa.gr (A. S. Kapoyannis), Vitalii.Ozvenchuk@ifj.edu.pl (V. Ozvenchuk), cnp@phys.uoa.gr ; president@cyi.ac.cy (C. N. Papanicolas), Andrzej.Rybicki@ifj.edu.pl (A. Rybicki), stiliaris@phys.uoa.gr (E. Stiliaris)

index) ϕ_2 . Using data-sets at different peripheralities, we also study the dependence of the ϕ_2 -value on the number of wounded nucleons, in order to uncover the approach to the critical point. With these findings and the help of Ising-QCD partition function, the interpretation of SPS intermittency measurements and their links to the critical region, are discussed.

Keywords: QCD phase diagram, critical region, proton intermittency, AMIAS, NA61/SHINE experiment

1. Introduction

During the last decade (2010-2020) a systematic search for QCD critical fluctuations was performed at the CERN SPS (NA49, NA61/SHINE) in measurements of intermittency in A + A collisions [2, 3, 4]. The aim was to capture critical fluctuations when the chemical freeze out of a particular collision comes close to the critical end point in the QCD phase diagram. This picture relies upon the experimental fact that chemical freeze out in A + A collisions is a state in thermal equilibrium and, therefore, universal fluctuations at the critical point, dependent on the static critical exponents, may, in principle, be revealed. In fact, intermittency in transverse momentum space, linked to the order parameter of the critical point (σ -field simulated by $\pi^+\pi^-$ pairs or net-baryon number) is a manifestation of finite size scaling, a fundamental property of critical systems [5, 6]. The formulation of intermittency along these lines leads to the following prediction at the critical point, for the two choices of the order parameter [7, 8]:

(a) density of $\pi^+\pi^-$ with zero effective mass (σ -field) \Rightarrow

$$\Delta F_2 \sim (M^2)^{\phi_2^{(\sigma)}} \quad ; \quad \phi_2^{(\sigma)} = 1 - \frac{2\beta}{3\nu},$$

(b) baryon-number density $\Rightarrow \Delta F_2 \sim (M^2)^{\phi_2^{(b)}} \quad ; \quad \phi_2^{(b)} = 1 - \frac{\beta}{3\nu}$

where ΔF_2 is a properly defined correlator, associated with scaled factorial moment F_2 [9], $\beta \approx \frac{1}{3}$, $\nu \approx \frac{2}{3}$ are 3d Ising critical exponents and M^2 the number of 2d bins in transverse momentum space.

Within this general framework, in a series of measurements performed by the SPS NA49 experiment, an analysis of nuclear reactions C + C, Si + Si and Pb + Pb at the maximum SPS energy concluded that:

- (a) there is no intermittency effect in the processes C + C and Pb + Pb, whereas
- (b) a sizeable intermittency effect with critical characteristics is observed in Si + Si, at maximum SPS energy with $\phi_2^{(\sigma)} \approx 0.35$, $\phi_2^{(b)} = 0.96_{-0.25}^{+0.38}$, compared to the QCD prediction $\phi_2^{(\sigma)} = \frac{2}{3}$, $\phi_2^{(b)} = \frac{5}{6}$ [2, 3].

In the successor to NA49, the SPS-NA61/SHINE experiment, measurements of proton intermittency in the reactions Be + Be, Ar + Sc at maximum SPS energy ($\sqrt{s_{NN}} = 16.8$ GeV) lead to the following preliminary results [4, 10, 11]: there is no intermittency effect either in Be + Be, or in Ar + Sc for extremely central collisions (0 – 5% most central) of the Ar + Sc reaction. However, a non zero effect was traced in peripherality 10 – 20% of the same reaction, [4, 11] reflecting possibly a small increase of freeze-out temperature with increasing peripherality due to a decrease of the fireball size [12, 13], bringing, presumably, the system closer to the critical region. Nevertheless, the interpretation of this result remains inconclusive since no reliable estimate of the exponent $\phi_2^{(b)}$ can be fixed, mainly due to the uncertainties induced by correlated bins and large statistical errors in the intermittency treatment [11, 14]. As a result, we notice that there exists a valuable compilation of SPS intermittency measurements which show a critical activity in the region of nuclear sizes A=30-40 at the maximum SPS energy of various A + A collisions, inconclusively interpretable due to the aforementioned uncertainties. In the present work, we make an attempt to understand the significance of these measurements in a phenomenological treatment, with complementary tools and theoretical ideas.

We employ a model-independent analysis scheme (AMIAS) in order to produce unbiased results for the parameters of the power laws and overcome the obstacle of correlated bins in the intermittency treatment [1, 14]. We also make use of the Ising-QCD partition function, close to the critical point [6], in order to discuss the location of the singularity and interpret the measurements in Ar + Sc at different centralities. Our description, along these lines, is organized as follows: In section 2, the general principles of the AMIAS method are presented, emphasizing the treatment of correlated data. In section 3, the AMIAS results for the intermittency parameters, limited to the measurements in Si + Si (0 – 12%) and Ar + Sc for varying centralities, are discussed. Also, the plot of ϕ_2 versus N_w (number of wounded nucleons) is constructed [15], illustrating the approach of NA61/SHINE freeze-out states,

towards the critical point. In section 4, the location of the SPS freeze-out states (NA49, NA61/SHINE) in the phase diagram is investigated with respect to the critical region. In particular, it is examined whether the AMIAS intermittent solutions are accommodated within the critical region or remain outside but close to the boundaries. This study becomes instrumental for the experimental estimate of the size of the critical region. Theoretically, the Ising-QCD partition function predicts a critical region that is a few MeV wide along the chemical potential direction [6]. Finally in section 5, our results and conclusions are summarized.

2. The AMIAS method

The AMIAS method [1, 16] has been developed in order to extract physical information from experimental or simulated data with the highest possible precision and in an unbiased way. It is based on statistical concepts and is able to handle a rather large number of parameters using Monte Carlo techniques. The method requires the definition of a theory or model which links the parameters to be determined in an explicit way with the data. Although AMIAS is well suited to resolve physical parameters from data where the underlying model cannot be inverted, it can equally well address simple fit cases with noisy data. Recently, AMIAS has been successfully applied in the analysis of pion photoproduction data for the extraction of the multipole excitation amplitudes [17] as well as in lattice QCD investigations for Tetraquark interpolating fields [18].

For a given set of parameters that defines the physical model, the principal idea behind AMIAS is that any arbitrary value assigned to the parameters constitutes a possible solution. Each of these solutions is weighted with a probability value retrieved out of the data set by a cost function. The information obtained from the given set of data is a Probability Density Function (PDF) assigned to each of the model parameters. The central values of the parameters and their uncertainties are therefore the expectation values and the standard deviations of the corresponding PDFs. The sampling method used in AMIAS allows all fit parameters to randomly vary and to yield solutions with all allowed values, including the insensitive exponential terms.

In the present work our aim is to use the AMIAS protocol for the detection of power-law behaviour in the density-density correlation function of protons in transverse momentum space for small transverse momentum

differences. This scenario is expected to be realized in protons produced in the central rapidity region in ion collisions, whenever the produced fireball freezes-out at the thermodynamic conditions (baryochemical potential, temperature) of the QCD critical point [8]. In fact, this effect is the momentum space counterpart of finite size scaling in configuration space [19] revealed through the Fourier transform of the real space density-density correlation function [20]. The relevant information is contained in the second order factorial moment F_2 counting the, properly normalized, mean number of proton pairs per transverse momentum space cell [21]. A given transverse momentum domain is partitioned into M^2 cells and F_2 is calculated for different values of M . The presence of power-law density-density correlations is reflected in the function $F_2(M)$ which in this case behaves, in the limit of large M , as $\sim M^{2\phi_2}$ where ϕ_2 is the intermittency index and the associated physical scaling effect is characterized as intermittency. In experimental data, the intermittency effect may be masked by the presence of noise, i.e. proton pairs which do not follow a power-law, or particles misidentified as protons. In addition, the fact that the values of $F_2(M)$ for different M s are correlated raises the question how these correlations affect the corresponding errors which are unavoidably present due to finite statistics. Before applying AMIAS to experimental data in the next section, we demonstrate here its power to overcome these difficulties.

For this purpose, we use a modified version of the Critical Monte-Carlo (CMC) event generator [22, 23] suited for simulating protons in transverse momentum space; simulated protons are produced through a truncated Lévy walk process to exhibit density-density correlations mimicking those originating from a fireball freezing out at the QCD critical point. The power-law exponent is chosen to describe correlations characterizing a critical system in the 3d-Ising universality class; associated intermittency index has the value $\phi_2 = \frac{5}{6}$ [8]. Furthermore, the algorithm can be parametrized [10] to produce an exponential one-particle proton p_T distribution and a Poissonian per-event proton multiplicity distribution, the values of which can be plugged in; finally, truncated Lévy walk bounds can be fine-tuned in order to produce critical density-density correlations within the desired scales.

A number of uncorrelated proton momenta drawn from a one-particle p_T distribution are interspersed among the critical protons at an adjustable percentage. These simulate the effect of non-critical background contamination on the critical signal.

In the following text, and unless stated otherwise, proton intermittency

analysis of $F_2(M)$ is applied within a rectangular region in transverse momentum space: $-1.5 \leq p_x, p_y \leq 1.5$ GeV/ c . The number M of one-dimensional bins in momentum space ranges from 1 to 150. The power-law fit for the intermittency index ϕ_2 is performed in the $M^2 \in [10^3, 10^4]$, or equivalently the $M \in [32, 100]$, range.

For our AMIAS test, we generate sets of ~ 400 K proton events with the characteristics of the NA61/SHINE Ar + Sc 10 – 20% most central data set at 150A GeV/ c beam momentum ($\sqrt{s_{NN}} = 16.8$ GeV). Average proton multiplicity per event is adjusted to ~ 2.5 , with a standard deviation of ~ 1.4 . Critical proton tracks are contaminated with 99.3% noise (0.7% critical component). This huge noise masks the underlying power-law behaviour at the level of $F_2(M)$. As shown in [3] in this regime, the power-law component is revealed in the correlator $\Delta F_2(M) \equiv F_{2,\text{data}}(M) - F_{2,\text{mixed}}(M)$, accounting for the subtraction of the background simulated by mixed events, $F_{2,\text{mixed}}(M)$. This behavior is evident in Fig.1 (left), where the pure and background-diluted CMC factorial moments are shown in double logarithmic scale: the correlator $\Delta F_2(M)$ retains the critical slope of the pure CMC $F_2(M)$, even though its values are reduced by orders of magnitude compared to pure CMC. Fig.1 (right) shows $\Delta F_2(M)$ for the same set of events, plotted against the distribution of $\Delta F_2(M)$ values for a total of 400 independent CMC sets, under the same conditions (linear scale is used to accommodate negative values). One observes that the original sample is typical, falling mostly within the central yellow band roughly corresponding to 1σ , whereas a minority of samples have either lower or higher slopes. However, in itself the distribution of $\Delta F_2(M)$ values does not give a complete picture of the power-law behaviour of moments due to the role of bin correlations.

The above generated sets have been analyzed with the AMIAS method. A total of 400 independent iterations with 150 data points each are assembled in a grand examination set. The function used to fit the data had the following analytical form

$$\Delta F_2(M) = 10^{a_0} \left(\frac{M^2}{10^4} \right)^{\phi_2} \quad (1)$$

where a_0 and ϕ_2 are the two fit parameters. The uniform sampling method has been applied in the Monte-Carlo technique choosing appropriate variation range for both parameters. Millions of possible solutions are selected by eliminating extreme values with the help of a χ^2 -cut. The final PDF solutions for the fit parameters are constructed in the usual way by weighting each

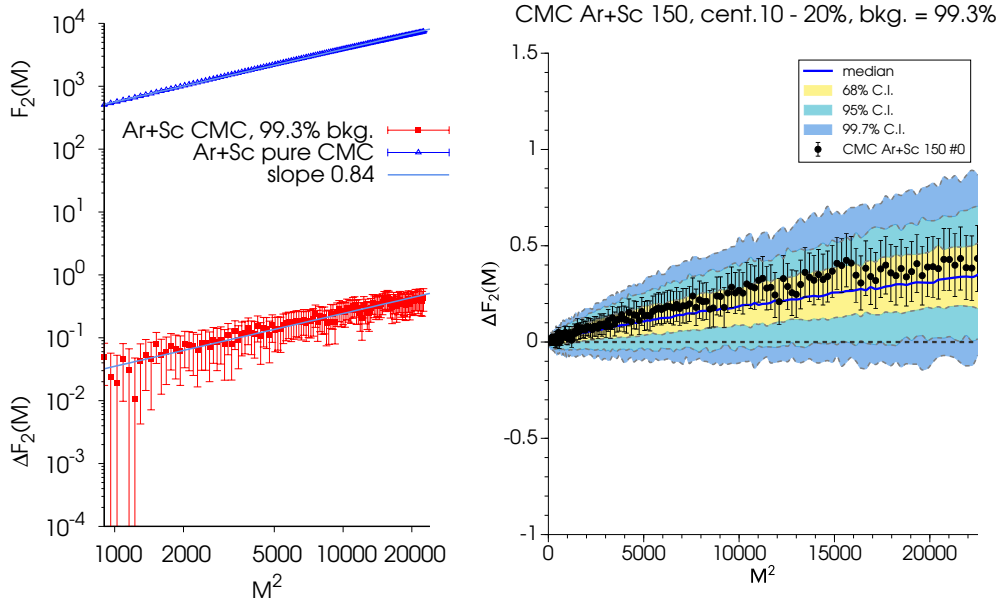


Figure 1: (Left) $F_2(M)$ of pure (blue triangles) and $\Delta F_2(M)$ of background-diluted CMC (red squares) Ar + Sc simulated collisions (10 – 20% most central, $\sqrt{s_{NN}} = 16.8$ GeV). Slope lines of $\phi_{2,cr} \simeq 0.84$ are fitted to both sets to guide the eye; (Right) $\Delta F_2(M)$ of background-diluted CMC for the same ~ 400 K event CMC iteration (black points & error bars), along with $\Delta F_2(M)$ confidence intervals (68-95-99.7%) for 400 independent iterations.

point of the accumulated sample with the factor $e^{-\chi^2/2}$.

The obtained PDFs for the two parameters a_0 and ϕ_2 are shown in Fig. 2 together with the microcanonical ensemble of both solutions. The extracted value for the power law parameter is $\phi_2 = 0.83 \pm 0.06$, which is in perfect agreement with the value used in the generator. Fig. 3 summarizes all generated CMC data sets with the AMIAS solution extracted from the central parameter values.

In the following, we will focus on the extraction of the power-law behaviour in $\Delta F_2(M)$ obtained from experimental data in NA49 and NA61/SHINE experiments.

3. Intermittent fluctuations in SPS (CERN)

In this section we employ AMIAS to estimate the intermittency index ϕ_2 based on the NA61/SHINE (CERN, SPS) preliminary measurements of the proton transverse momentum space correlator ΔF_2 in Ar + Sc collisions at 150A GeV/c beam momentum for different peripheralities in the range 0 – 20% [11]. Our goal is to explore how the associated ϕ_2 distribution, determined by AMIAS, depends on peripherality of the collisions. As mentioned also in the Introduction, such a study is twofold motivated:

- Freeze-out states produced in Ar + Sc collisions at 150A GeV/c beam momentum are expected to lie, in the baryochemical potential (μ_B) and temperature (T) plane, relatively close to $(\mu_{B,Si}, T_{Si})$, parametrizing the freeze-out state produced in central Si + Si collisions at 158A GeV/c (NA49 experiment at CERN-SPS). In the latter system intermittent fluctuations with critical characteristics have been observed [2, 3].
- The theoretical prediction that the critical region is very narrow in (μ_B, T) plane [19], implies that the neighbourhood of $(\mu_{B,Si}, T_{Si})$ should be explored with small steps in μ_B and T . Such a fine search can be realized in a suitable scan, employing freeze-out states of Ar + Sc collisions at 150A GeV/c at different peripheralities. This is due to the fact that there is experimental evidence as well as theoretical understanding [12, 13] that changes in the peripherality influence the freeze-out conditions (μ_B, T) in a prescribed mild manner.

In fact it is expected that more peripheral Ar + Sc collisions can approach the freeze-out conditions of central Si + Si collisions at similar energy. Unfortunately, experimental limitations restrict the range of peripherality variation

CMC Ar+Sc 150, AMIAS Results

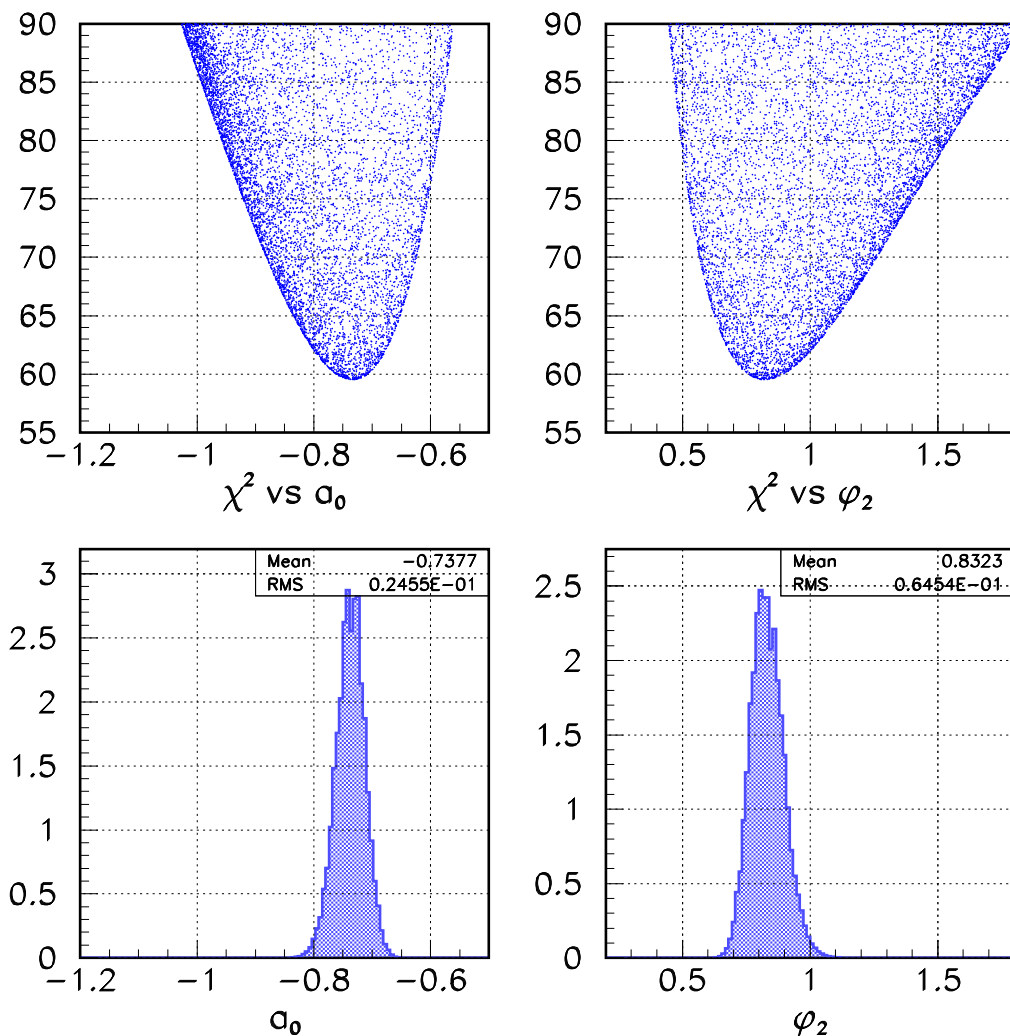


Figure 2: AMIAS results for the two fit parameters a_0 and ϕ_2 from the CMC generated 400 independent iterations. Top row (scatter plot) shows the microcanonical solution for each parameter. The histograms in the bottom row represent the non-normalized PDF solutions for both fit parameters.

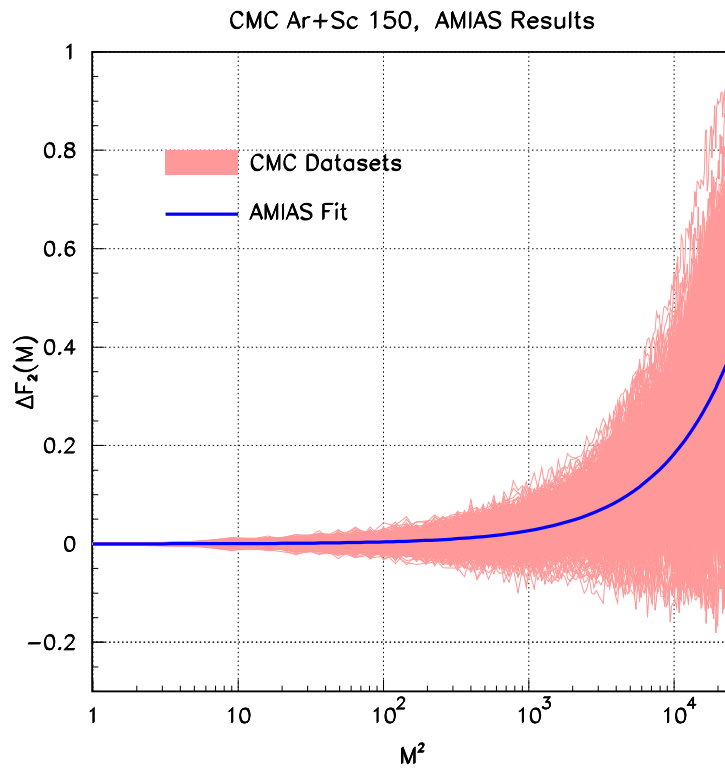


Figure 3: The AMIAS solution (line) extracted from the central parameter values together with all generated CMC data sets represented here as a colored band.

in the interval $0 - 20\%$. Within these constraints the NA61/SHINE experiment has measured the correlator ΔF_2 for Ar + Sc collisions at 150A GeV/c in different peripherality zones of increasing resolution. Starting from the coarsest scale $0 - 20\%$, the $0 - 20\%$ zone is subsequently partitioned into two non-overlapping intervals of 10% width, i.e. $0 - 10\%$ and $10 - 20\%$, and the resolution is further increased through a subdivision into four non-overlapping intervals of 5% width each: $0 - 5\%$, $5 - 10\%$, $10 - 15\%$ and $15 - 20\%$ providing the finest scale in this analysis. In Fig. 4(a-d) we present, indicatively, $\Delta F_2(M)$ plots for the peripheralities: (a) $0 - 20\%$, (b) $10 - 20\%$, (c) $10 - 15\%$ and (d) $15 - 20\%$. The remaining ΔF_2 measurements at peripheralities $0 - 10\%$, $0 - 5\%$ and $5 - 10\%$ are not shown here; we refer the interested reader to [11] for a detailed presentation.

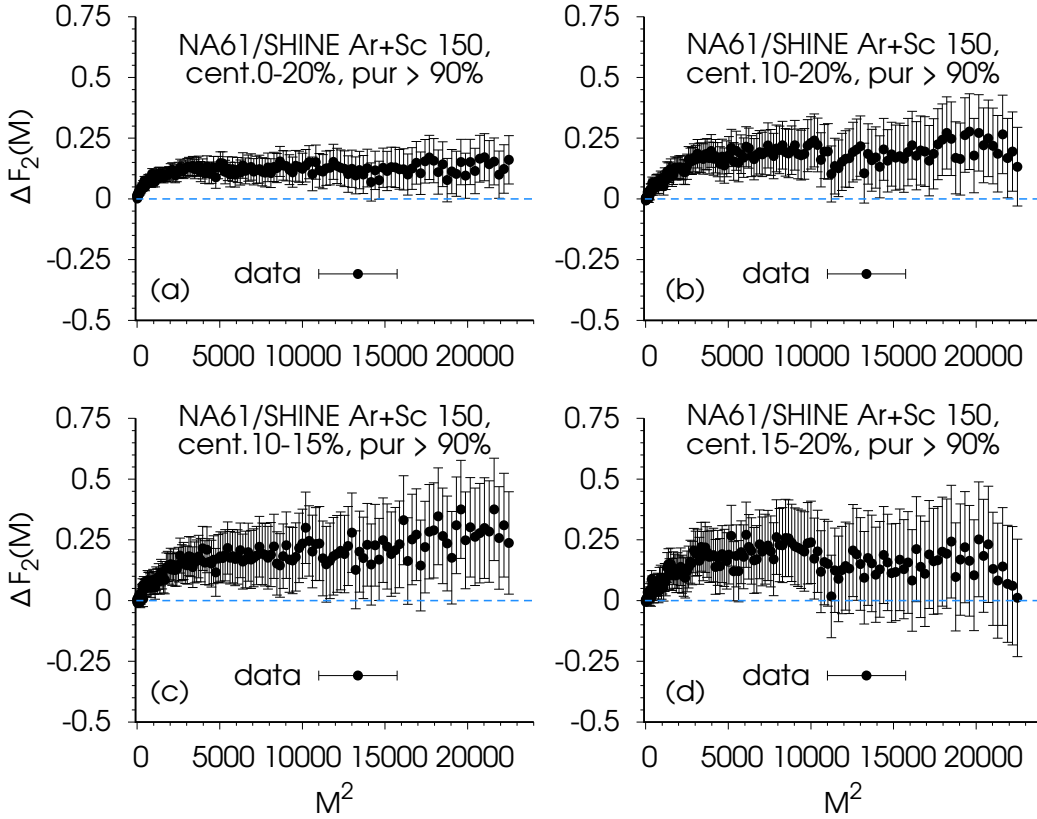


Figure 4: $\Delta F_2(M)$ for NA61/SHINE Ar + Sc (a) $0 - 20\%$, (b) $10 - 20\%$, (c) $10 - 15\%$, and (d) $15 - 20\%$ most central collisions at 150A GeV/c. Error bars correspond to statistical errors estimated via the bootstrap method [24, 25].

We use the AMIAS protocol to estimate the distribution of the intermittency index ϕ_2 for each of the cases described above. The results of this analysis are presented in two figures. In Fig. 5(a-d) we present the ϕ_2 -distribution for the corresponding cases for ΔF_2 shown in Fig. 4(a-d) while in Fig. 6(a-c) we show the ϕ_2 -distribution corresponding to the second set of NA61/SHINE ΔF_2 results concerning the 0 – 10%, 0 – 5% and 5 – 10% peripherality zones respectively.

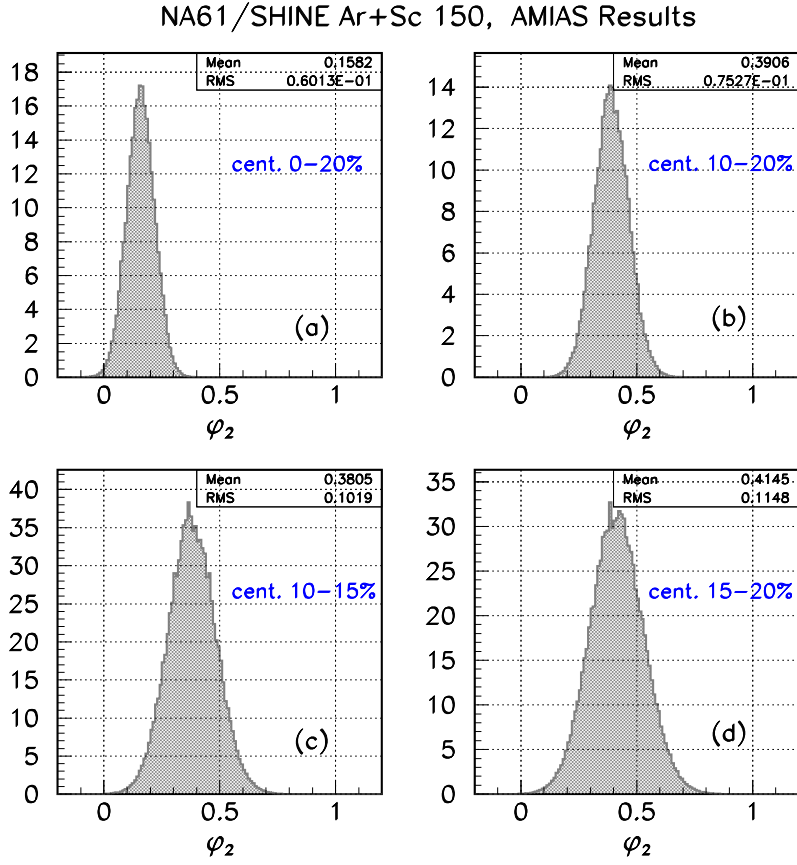


Figure 5: AMIAS analysis results for the ϕ_2 -distribution for the corresponding cases for ΔF_2 shown in Fig. 4(a-d).

We observe in Figs. 6(a-c) that no intermittency effect is detected in the peripherality bins 0 – 10% (and consequently also in the subdivisions 0 – 5% and 5 – 10%) while a clear intermittency effect, expressed by a non-vanishing mean ϕ_2 value and a standard deviation sufficiently small to exclude the

NA61/SHINE Ar+Sc 150, AMIAS Results

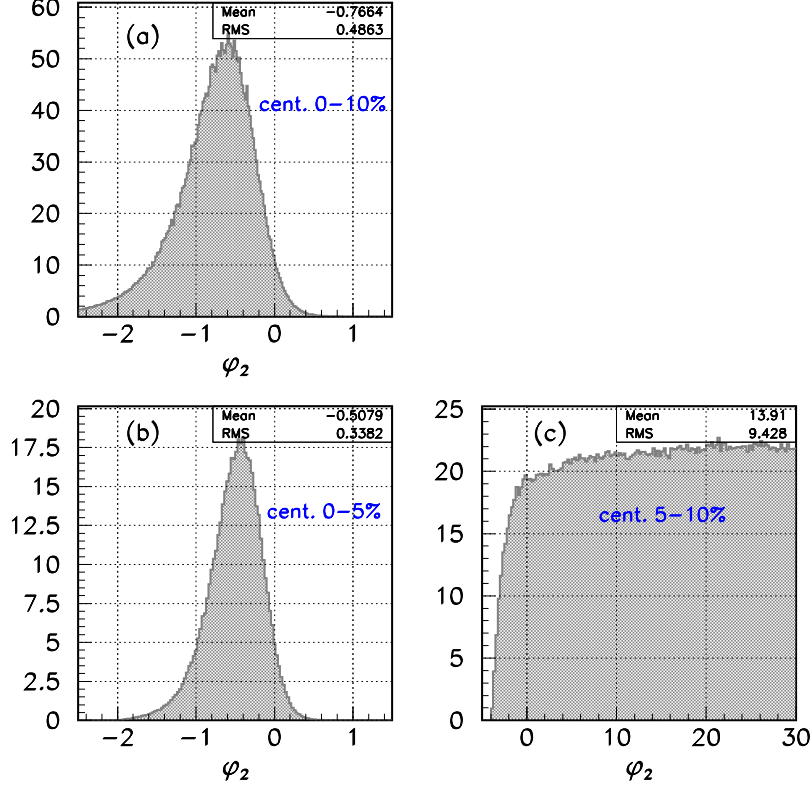


Figure 6: AMIAS analysis results for the ϕ_2 -distribution corresponding to the second set of NA61/SHINE ΔF_2 results concerning the 0 – 10%, 0 – 5% and 5 – 10% peripherality zones.

$\phi_2 \leq 0$ region, is observed in the peripherality bin 10 – 20%, as well as its subdivisions 10 – 15% and 15 – 20%, shown in Figs. 5(a-d). The mean value $\langle \phi_2 \rangle$ is slightly increased in the 15 – 20% as compared to that in the 10 – 15% peripherality interval. On average, in the 0 – 20% zone, a small but certainly non-vanishing intermittency effect is sustained. These results are compatible with a tendency of the Ar + Sc freeze-out state to approach the Si + Si freeze-out state with increasing peripherality. This behaviour was theoretically foreseen in [19].

For completeness we have used AMIAS to determine the distribution of the intermittency index ϕ_2 also for the Si + Si system analysed in detail in [3]. In Fig. 7a we show the correlator - for protons in transverse momentum

space - $\Delta F_2(M)$ (Si + Si collisions, peripherality 0 – 12%, 158A GeV/c) as measured in the NA49 experiment (SPS, CERN), while in Fig. 7b, we display the ϕ_2 distribution obtained with AMIAS. For consistency, we have used in AMIAS the same fitted M^2 -range as in [3], $M^2 \in [6000, 22500]$. The overall form of the distribution is compatible with the result published in [3]. The advantage of the AMIAS method is that it leads to a significantly narrower distribution than that obtained by applying the bootstrap method [24, 25] to ϕ_2 fits, as detailed in [3].

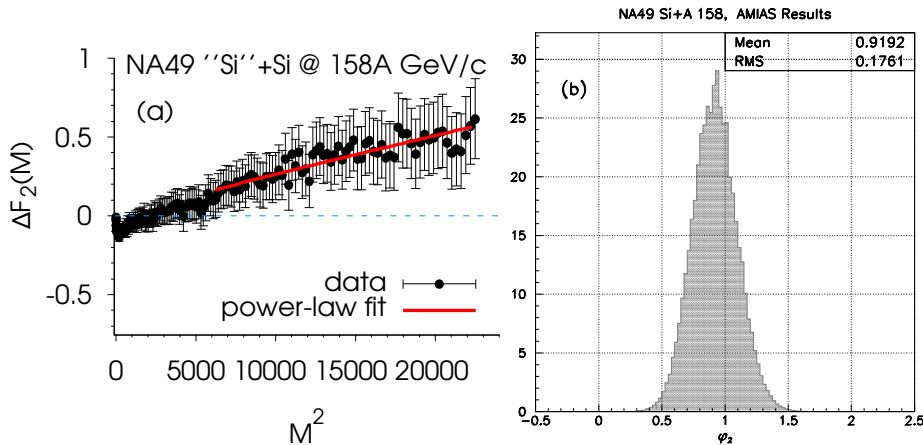


Figure 7: *Left:* $\Delta F_2(M)$ for NA49 Si + Si 0-12% most central collisions at 158A GeV/c [3]. *Right:* AMIAS distribution for the intermittency index ϕ_2 .

A transparent interpretation of the results shown in Figs. (5-7) is possible if one uses the number of wounded nucleons N_w for the characterization of the freeze-out states associated with each peripherality bin.

The mean number of wounded nucleons in each bin of Ar + Sc collisions is estimated by means of a geometrical Glauber simulation [26]. The Ar nuclear density profile is obtained from the Fourier-Bessel expansion of the nuclear charge density [27] while the Sc profile is taken as a Saxon-Woods distribution with half density and surface thickness terms taken as 0.542 fm and 3.77 fm, respectively [27, 28]. The nucleon-nucleon cross-section at this energy is taken as 31.42 mb in agreement with literature [29]. In order to match the specific NA61/SHINE centrality selection based on the energy deposit in a forward calorimeter [30], the simulated centrality samples are defined by the energy of projectile (Ar) spectator nucleons. The potential influence of the additional energy deposit by produced charged particles in

the NA61/SHINE forward calorimeter can be deduced from Ref. [31] and it is included in the uncertainty estimated for our calculation, presented in Table 1.

In Table 1 we summarize the results of the AMIAS analysis in the considered systems, presenting the mean value $\langle\phi_2\rangle$ as well as the corresponding error $\delta\phi_2$ obtained from the ϕ_2 distributions in Figs. (5-7), providing also the estimated N_w value for each analysed data set.

Reaction	centrality (%)	N_w	$\langle\phi_2\rangle$ ($\delta\phi_2$)
Ar + Sc	0-10	62(0.6)	-0.77(49)
Ar + Sc	10-20	45.9(0.5)	0.39(08)
Ar + Sc	0-5	66.6(0.9)	-0.51(34)
Ar + Sc	5-10	57.3(0.4)	–
Ar + Sc	10-15	49.4(0.4)	0.38(10)
Ar + Sc	15-20	42.4(0.5)	0.41(12)
Ar + Sc	0-20	54(0.6)	0.16(06)
Si+A	0-12	37(3)	0.92(18)

Table 1: AMIAS $\langle\phi_2\rangle$ and corresponding error $\delta\phi_2$ results vs the estimated mean number of wounded nucleons N_w for central Si + Si and different Ar + Sc peripherality ranges.

It is interesting to plot the intermittency index ϕ_2 , calculated with AMIAS, as a function of the number of wounded nucleons, similarly to the plot presented in [15] using ϕ_2 -values obtained through ordinary fitting procedure. In Fig. 8 we show such a plot including only systems with $N_w < 55$. Since N_w is a quantity related to the effective size of the produced fireball, it is expected to depend smoothly on the freeze-out temperature T [32]. We clearly observe the tendency of the most peripheral Ar + Sc freeze-out states to approach the Si + Si freeze-out state since N_w is decreasing with increasing peripherality. It is remarkable that, at the same time, the intermittency index ϕ_2 increases too, indicating the proximity to the critical region. Clearly the ϕ_2 value for the freeze-out state associated with the most peripheral Ar + Sc collisions is still far from the critical value (0.41 compared to 0.83) indicating that this system has not entered yet into the critical region [19]. Furthermore, the absence of an intermittency effect in the C + C (central collisions at 158A GeV/c, NA49) [3] and Be + Be (central collisions at 150A GeV/c, NA61/SHINE preliminary) [10] systems with $N_{w,C} \approx 14 < N_{w,Si} \approx 37$ [32],

implies the formation of a maximum located close to $N_w = N_{w,S_i}$ in the $\phi_2(N_w)$ function. Unfortunately, due to very low proton multiplicity and insufficient statistics the ϕ_2 value for Be + Be is indeterminable. Nevertheless, the overall picture provides us with a rough estimation of the size of the critical region quantified by the differences $|\phi_2 - \frac{5}{6}|$ and $|N_w - N_{w,S_i}|$. A more detailed representation of the critical region and its surroundings requires additional theoretical tools and it will be presented in the next section. There we will show that, in the immediate neighbourhood of the critical point, the quantities ϕ_2 and N_w form an almost cartesian coordinate system, allowing an alternative parametrization of the QCD phase diagram in this region.

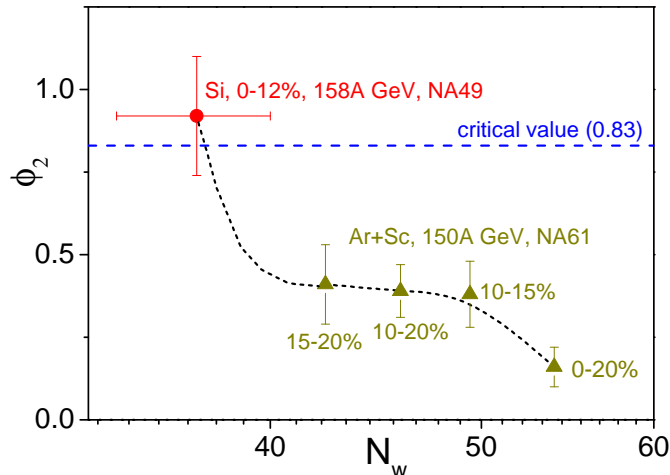


Figure 8: The intermittency index ϕ_2 versus the number of wounded nucleons N_w for the systems: Si + Si at 158A GeV/c and periphery 0 – 12% (NA49 experiment, red circle), Ar + Sc at 150A GeV/c and peripheralities 0 – 20%, 10 – 20%, 10 – 15% and 15 – 20% (NA61/SHINE experiment, light green triangles). The dashed blue line indicates the critical ϕ_2 value $\phi_{2,cr} = \frac{5}{6}$.

4. Probing the QCD critical region

In this section we exploit the AMIAS results of the previous section to construct a phase diagram of the critical region and its surroundings along

the lines introduced in [19]. To this end we employ the Ising-QCD partition function \mathcal{Z} , derived in [6], to describe the net-baryon density and its fluctuations close to the critical point. To be self-contained, we repeat here the definition of \mathcal{Z} :

$$\mathcal{Z} = \sum_{N=0}^L \zeta^N \exp \left[-\frac{1}{2} \hat{m}^2 \frac{N^2}{L} - g_4 \hat{m} \frac{N^4}{L^3} - g_6 \frac{N^6}{L^5} \right] \quad (2)$$

where $N = N_B - N_{\bar{B}}$ is the net-baryon number in volume $V = L\beta_c^3$, $\beta_c = 1/k_B T_{cr}$ being the characteristic length scale of the system fixed by the critical temperature T_{cr} . The dimensionless variable L quantifies the size of the considered baryonic system. The universal couplings $g_4 = 0.97 \pm 0.02$, $g_6 = 2.05 \pm 0.15$ are calculated in [33] while $\hat{m} = \beta_c m$ is related to the correlation length $\xi = m^{-1}$ of the infinite system, given by $\xi = \xi_{0,\pm} |t|^{-\nu}$ with $\nu \approx \frac{2}{3}$ for the 3d Ising universality class and $t = \frac{T - T_{cr}}{T_{cr}}$ the reduced temperature. The index \pm in $\xi_{0,\pm}$ is used to distinguish between the region $T > T_{cr}$ in which the correlation length amplitude is $\xi_{0,+}$ and the region $T < T_{cr}$ where the corresponding amplitude is $\xi_{0,-}$. Notice that the ratio $\frac{\xi_{0,+}}{\xi_{0,-}}$ is fixed and approximately equal to 2 in the 3d-Ising universality class. Finally, $\zeta = e^{(\mu_B - \mu_{B,cr})\beta_c}$ represents the fugacity in the grand canonical ensemble with $\mu_{B,cr}$ the critical baryochemical potential. As explained in [19] Eq. (2) provides a valid thermodynamic description of the critical fluid in the neighbourhood of the critical point where hadronic and quark phases are indiscernible. Furthermore, the partition function (2) reproduces accurately all the critical properties, i.e. scaling, critical exponents, of the 3d Ising system [34]. It can be used to derive scaling laws of the form:

$$\langle N^k \rangle \sim L^{kq}, k = 1, 2, \dots \quad (3)$$

expressing the finite size scaling properties of the critical fluid [19]. For the 3d-Ising model the power-law exponent is $q \approx \frac{5}{6}$. In fact, the partition function (2) enables also the description of the baryonic fluid for thermodynamic conditions close, but at a distance from the critical point $(\mu_{B,cr}, T_{cr})$. In such a case, scaling laws of the form in Eq. (3) are still approximately valid, however the exponent q is modified to \tilde{q} varying in the range $[0, \frac{5}{6})$ or $(\frac{5}{6}, 1]$. Then, the difference $|\tilde{q} - \frac{5}{6}|$ provides a measure for the distance from the critical baryochemical potential value μ_c , as shown in [19]. Of course, far from the critical point the validity of the partition function \mathcal{Z} in (2) breaks down. The

importance of the power-law exponent \tilde{q} is that it can be measured in ion collision experiments through intermittency analysis in transverse momentum space. Within this framework, power-law behaviour of the correlator $\Delta F_2(M) \sim M^{2\phi_2}$ as a function of the number of cells M in transverse momentum space partitioning (intermittency effect), is a manifestation of the finite-size scaling (3) in configuration space, both effects related to each other through a Fourier transform [20]. As a consequence the intermittency index ϕ_2 coincides with the finite-size scaling exponent q (or more general \tilde{q}).

For the construction of the phase diagram we will use two basic ingredients: (i) the ϕ_2 values calculated with AMIAS and (ii) the number of wounded nucleons N_w calculated with a geometrical Glauber model simulation [26]. For both quantities we will use their central values, given in Table 1, neglecting the associated errors. However, the essentials of our treatment, contained in the methodological approach, are in general valid independently of this choice. Initially the phase diagram will be presented in the reduced variables $\ln \zeta$ (reduced baryochemical potential) and t (reduced temperature), however, as we will see in the following, close to the critical point the quantities ϕ_2 and N_w play a similar role.

Our strategy is as follows:

- Firstly we determine the curves $\phi_2(\ln \zeta, t) = C_i$ with $i = 1, 2, \dots, 5$ and C_i constant values taken from the last column in Table 1 in increasing order. We consider only the cases with $C_i > 0$.
- Subsequently we construct the corresponding $N_w(\ln \zeta, t) = c_i$ curves (with $i = 1, \dots, 5$) where the c_i values are taken from the third column in Table 1.
- The intersections of these families of lines determine the location of the corresponding freeze-out states in the $(\ln \zeta, t)$ plane.

To achieve the first task, we employ Eq. (2) for the calculation of the function $\langle N \rangle(L)$ at each point of a 401×401 grid in the $(\ln \zeta, t)$ plane. The grid covers the region $\ln \zeta \in [-0.12, 0.12]$ and $t \in [-0.2, 0.2]$. The variable L , being the ratio of the volume of the entire system (fireball) to the volume of a single nucleon, varies in the range $30 \leq L \leq 700$, corresponding to nuclei with linear size from 3 to 9 fm. This range of L values covers all experimentally accessible cases from small to medium size nuclei in NA49 and NA61/SHINE experiments.

We perform a linear fit in the function $\ln\langle N \rangle(\ln L)$ at each point of the $(\ln \zeta, t)$ grid and we check its validity with the regression coefficient R^2 setting the constraint $R^2 \geq 70\%$ for the characterization as a power-law. The slope parameter of this fit provides us the ϕ_2 -value at each grid point. The set of $(\ln \zeta, t)$ points leading to the same ϕ_2 value, within a $\pm 10^{-3}$ -deviation, determines the curve with constant ϕ_2 in the $(\ln \zeta, t)$ plane.

The results of this calculation are shown in Fig. 9a. The red lines in this plot correspond to $\phi_2 = 0.75$ (left) and $\phi_2 = 1$ (right) determining the borders of the critical region (red shaded area), according to the definition given in [6]. The blue curve is associated with the ϕ_2 value for the Si + Si system ($\phi_{2,Si} = 0.92$) while the green curves correspond to the ϕ_2 values found for Ar + Sc in the peripherality zones 10 – 20%, 10 – 15% and 15 – 20%, while the orange curve displays the $\phi_2 = 0.16$ curve (Ar + Sc, peripherality 0 – 20%). For all cases, a piecewise linear description of the $\phi_2(\ln \zeta, t) = \text{constant}$ curve is a good approximation. Notice, that all curves of constant ϕ_2 -values in Fig. 9a, being expressed in reduced variables, do not depend on the specific $(\mu_{B,cr}, T_{cr})$ -values. Thus, the displayed pattern is universal, characterizing the 3d Ising class.

In particular, the information contained in the blue curve in Fig. 9a can be further exploited, when combined with the results plotted in Fig. 8, as well as the data for the freeze-out baryochemical potential $\mu_{B,Si}$ and temperature T_{Si} of the Si + Si system, estimated with the statistical hadronization model in [12]. In fact, it allows the determination of the critical baryochemical potential $\mu_{B,cr}$ as a function of the critical temperature T_{cr} , following the line of thought given below:

- Fig. 8 dictates that the critical temperature is slightly below the freeze-out temperature of the Si + Si system, since the function $T(N_w)$ is decreasing [12, 13]. This means that the freeze-out state of Si + Si must lie on the upper branch of the blue curve in Fig. 9a where $t_{Si} = \frac{T_{Si} - T_{cr}}{T_{cr}} > 0$.

- The upper branch of the blue curve in Fig. 9a can be described by the line:

$$t = a_{Si} \ln \zeta + b_{Si} \quad ; \quad a_{Si} = 47.52 \quad ; \quad b_{Si} = -0.36 \quad (4)$$

obtained by fitting.

- For given $\mu_{B,Si}$ and T_{Si} , equation (4) provides a relation between $\mu_{B,cr}$

and T_{cr} :

$$\mu_{B,cr} = \mu_{B,Si} + \frac{(1 + b_{Si})T_{cr} - T_{Si}}{a_{Si}} \quad (5)$$

taking into account that $\ln \zeta_{Si} = \frac{\mu_{B,Si} - \mu_{B,cr}}{k_B T_{cr}}$.

- In [12] it is found that $\mu_{B,Si} = 260 \pm 17.9$ MeV and $T_{Si} = 162.2 \pm 7.9$ MeV. Using the central values $(\mu_{B,Si}, T_{Si}) = (260, 162.2)$ MeV and assuming $T_{cr} = 162$ MeV, we find $\mu_{B,cr} = 258.8$ MeV. Although this is an indicative result obtained neglecting errors, the described procedure can be used for any set of $\{\mu_{B,Si}, T_{Si}, T_{cr}\}$ values to determine $\mu_{B,cr}$. Notice that the choice $T_{cr} = 162$ MeV is compatible with some recent Lattice QCD results [35].

In the second step we place the curves $N_w(\ln \zeta, t) = c_i$ ($i = 1, \dots, 5$) on the $(\ln \zeta, t)$ -plane. We assume, therefore, a lowest order expansion of the function $N_w(\ln \zeta, t)$ around $(\ln \zeta_{Si}, t_{Si})$ of the form:

$$N_w(\ln \zeta, t) = N_w(\ln \zeta_{Si}, t_{Si}) + \gamma_t(t - t_{Si}) + \gamma_\zeta(\ln \zeta - \ln \zeta_{Si}) \quad (6)$$

with $N_w(\ln \zeta_{Si}, t_{Si}) = 37$ (see Table 1) and γ_t, γ_ζ constants to be determined. Notice that, according to Fig. 8 (and Table 1), the number of wounded nucleons $N_{w,cr}$ at the critical point $(\ln \zeta_{cr}, t_{cr}) = (0, 0)$ is bounded in the range $37 \leq N_{w,cr} < 42.4$. Therefore it is convenient, if possible, to parametrize the constants γ_t and γ_ζ in Eq. (6) in terms of $N_{w,cr}$. To this end, we use the freeze-out state $(\ln \zeta_C, t_C)$ formed in central C + C collisions at 158A GeV/c (NA49, CERN), which lies close enough to the Si + Si freeze-out state [12] to obey Eq. (6). We obtain the system of equations:

$$N_{w,cr} = N_{w,Si} - \gamma_t t_{Si} - \gamma_\zeta \ln \zeta_{Si} \quad (7a)$$

$$N_{w,C} = N_{w,Si} + \gamma_t(t_C - t_{Si}) + \gamma_\zeta(\ln \zeta_C - \ln \zeta_{Si}) \quad (7b)$$

with $N_{w,Si} = N_w(\ln \zeta_{Si}, t_{Si})$ and $N_{w,C} = N_w(\ln \zeta_C, t_C)$ respectively. Eqs. (7a,7b) can be solved for γ_t and γ_ζ yielding:

$$\gamma_t = \frac{N_{w,Si} - N_{w,cr} - \gamma_\zeta \ln \zeta_{Si}}{t_{Si}} \quad (8a)$$

$$\gamma_\zeta = \frac{t_{Si}(N_{w,C} - N_{w,Si}) + (t_C - t_{Si})(N_{w,cr} - N_{w,Si})}{t_{Si}(\ln \zeta_C - \ln \zeta_{Si}) - \ln \zeta_{Si}(t_C - t_{Si})} \quad (8b)$$

In Eqs. (8a,8b) $N_{w,Si}$ and $N_{w,C}$ are given in [32] while t_{Si} , $\ln \zeta_{Si}$, t_C and $\ln \zeta_C$ are determined by the values of T_{Si} , $\mu_{B,Si}$, T_C and $\mu_{B,C}$ given in [12] provided that T_{cr} and $\mu_{B,cr}$ are known. In consistency with the analysis in the first step we will use only the central values of [12] for T_{Si} , $\mu_{B,Si}$, T_C and $\mu_{B,C}$ (neglecting errors).

Furthermore, $\mu_{B,cr}$ can be expressed in terms of T_{cr} via Eq. (5). Thus, the only unknown parameters are T_{cr} and $N_{w,cr}$. Their values determine the lines $N_w = \text{constant}$. In Fig. 9a we show as an example the line $N_w = 37$ (dotted blue) assuming $T_{cr} = 156$ MeV and $N_{w,cr} = 39.5$. According to Table 1 this line corresponds to the Si + Si system. The intersection of this line with the curve $\phi_2 = 0.92$ determines the location of the Si + Si freeze-out state in the $(\ln \zeta, t)$ plane. The blue arrow is used to clarify this. In a similar way we can find the locations of the freeze-out states for the Ar + Sc systems at different peripheralities. They depend strongly on the chosen values T_{cr} and $N_{w,cr}$. Varying T_{cr} and $N_{w,cr}$ the slope $-\frac{\gamma_\zeta}{\gamma_t}$ of the lines $N_w = \text{constant}$ changes. A more quantitative description of this dependence is displayed in Fig. 9b where we plot $-\frac{\gamma_\zeta}{\gamma_t}$ as a function of $N_{w,cr}$ for different values of T_{cr} . We observe that this dependence becomes smoother, in the sense that the slope $-\frac{\gamma_\zeta}{\gamma_t}$ becomes smaller, for $T_{cr} = 162$ MeV. In the following considerations we will exclusively use this value for the critical temperature. With this choice, the data used to calculate the constants γ_t and γ_ζ get the values summarized in Table 2.

A + A	N_w	(μ_B, T) (MeV)	$(\ln \zeta, t)$	$\mu_{B,cr}$ (MeV)	T_{cr} (MeV)
C + C	14	(262.6,166)	(0.0235,0.0247)		
Si + Si	37	(260,162.2)	(0.007,0.001)	258.8	162

Table 2: Calculation of constants γ_t , γ_ζ for the choice of $T_{cr} = 162$ MeV.

The entries of Table 2 determine the constants γ_t , γ_ζ in terms of $N_{w,cr}$ as:

$$\gamma_t = -4833.9 + 100.8N_{w,cr} \quad ; \quad \gamma_\zeta = 5631.9 - 147.4N_{w,cr} \quad (9)$$

Then, it is straightforward to obtain the lines of constant value of N_w in the $(\ln \zeta, t)$ plane using Eq. (6), after choosing $N_{w,cr} \in [37, 42.4)$.

Especially interesting, from the phenomenological point of view, is the case where N_w is independent of $\ln \zeta$. Such a behaviour is also suggested by experimental data [12, 13]. Within our analysis, this scenario implies that

γ_ζ in Eq. (8b) vanishes, leading to the condition:

$$N_{w,cr} = N_{w,Si} + \frac{(T_{Si} - T_{cr})(N_{w,Si} - N_{w,C})}{T_C - T_{Si}} \quad (10)$$

which connects the critical temperature T_{cr} with the number of wounded nucleons at the critical point $N_{w,cr}$. For $T_{cr} = 162$ MeV we find, using Eq. (10), $N_{w,cr} = 38.2$. Using this value for $N_{w,cr}$ we show in Fig. 9c the critical region and its neighbourhood in the $(\ln \zeta, \phi_2)$ -plane. The location of the Ar + Sc freeze-out states for different peripheralities (NA61/SHINE experiment) in the interval 10 – 20% is shown by the green circles in this plot. The blue star displays the location of the Si + Si freeze-out state, while, for completeness, we include in the graph also the C + C freeze-out state (black star), both measured in NA49 experiment. The red circle indicates the location of the critical point. Finally the orange cross presents the freeze-out state of Ar + Sc in 0 – 20% peripherality interval. It is remarkable that the freeze-out states of the different systems are concentrated close to the critical point along the reduced temperature axis. At this scale the $\phi_2 = \text{constant}$ curves appear as almost vertical lines forming, together with the horizontal $N_w = \text{constant}$ (dotted coloured) lines a cartesian coordinate system for the description of the critical region and its neighbourhood.

Within this parametrization a nice interpretation is possible: the number of wounded nucleons N_w defines the temperature of a freeze-out state within and close to the critical region while the intermittency index ϕ_2 defines the corresponding baryochemical potential. As already discussed, small changes in the T_{cr} and in the T_{Si} , $\mu_{B,Si}$, T_C , $\mu_{B,C}$ values will not alter the form of the critical neighbourhood shown in Fig. 9c since the plot is in relative (reduced) coordinates with respect to the critical point. Thus, similarly to Fig. 9a, also Fig. 9c is a rather universal result. It indicates clearly the proximity to the critical region of the peripheral Ar + Sc collisions. However, within the peripherality range 0 – 20%, allowed by the NA61/SHINE experiment, the recorded freeze-out states are still at a distance from the critical region and therefore the observed intermittency effect [11] can not be characterized as critical. Nevertheless, together with NA49 intermittency results [2, 3], the NA61/SHINE intermittency analysis provides a close frame of the critical region.

5. Summary and conclusions

Employing the AMIAS method to extract the distributions of the intermittency index ϕ_2 from the preliminary NA61/SHINE results for the proton correlator $\Delta F_2(M)$ in transverse momentum space of the Ar + Sc system (150A GeV/ c beam momentum) at different peripheralities [11], we demonstrate the presence of a non-vanishing intermittency effect in the 10 – 20% peripherality interval. The AMIAS method of analysis is also applied to the $\Delta F_2(M)$ measurement in Si + Si central collisions (0 – 12% peripherality) at 158A GeV/ c by the NA49 experiment [3], verifying the presence of critical fluctuations in this system. The AMIAS results for ϕ_2 , combined with an estimation of the corresponding number of wounded nucleons N_w for each considered freeze-out state, allow the mapping of the critical region and its neighbourhood in the reduced baryochemical-temperature plane, in terms of the quantities ϕ_2 and N_w . This mapping indicates that the preliminary NA61/SHINE intermittency results are fully compatible with the corresponding NA49 measurements reflecting transparently the approach of the Ar + Sc freeze-out states towards the critical region with increasing peripherality. Our analysis provides strong constraints on the location of the critical region and it may be used as an invaluable guide in the forthcoming experimental searches for the QCD critical point.

Acknowledgments: This work was supported by the National Science Centre, Poland (grant no. 2014/14/E/ST2/00018).

References

- [1] C. N. Papanicolas, E. Stiliaris, arXiv:1205.6505 (2012).
- [2] T. Anticic *et al.*, Phys. Rev. C **81**, 064907 (2010).
- [3] T. Anticic *et al.*, Eur. Phys. J. C **75**, 587 (2015).
- [4] M. Mackowiak-Pawłowska [NA61/SHINE Collaboration], arXiv:2002.04847 [nucl-ex].
- [5] H. Meyer-Ortmanns, Rev. Mod. Phys. **68**, 473 (1996).
- [6] N. G. Antoniou, F. K. Diakonou, X. N. Maintas and C. E. Tsagkarakis, Phys. Rev. D **97**, 034015 (2018).

- [7] F. K. Diakonou, N. G. Antoniou and G. Mavromanolakis, PoS **CPOD 2006**, 010 (2007).
- [8] N. G. Antoniou, Y. F. Contoyiannis, F. K. Diakonou and C. G. Papadopoulos, Phys. Rev. Lett. **81**, 4289 (1998).
- [9] N. Davis, “*Searching for the chiral critical point of quark matter in relativistic ion collisions*” (PhD thesis), <http://hdl.handle.net/10442/hedi/36113>.
- [10] N. Davis [NA61/SHINE Collaboration], N. G. Antoniou and F. K. Diakonou, PoS **CPOD 2017**, 054 (2018).
- [11] N. Davis [NA61/SHINE Collaboration], arXiv:2002.06636 [nucl-ex].
- [12] F. Becattini, J. Manninen, M. Gazdzicki, Phys. Rev. C **73**, 044905 (2006).
- [13] F. Becattini, M. Bleicher, E. Grossi, J. Steinheimer and R. Stock, Phys. Rev. C **90**, 054907 (2014).
- [14] C. Michael, Phys. Rev. D **49**, 2616 (1994).
- [15] S. Pulawski [NA61/SHINE Collaboration], “*Status and plans of the NA61 Experiment*,” News from the Experiments at CERN (131st Meeting of the SPSC), 16-17 October 2018, <https://indico.cern.ch/event/758114/>.
- [16] E. Stiliaris, C. N. Papanicolas, AIP Conf. Proc. **904**, 257 (2007).
- [17] L. Markou, E. Stiliaris, C. N. Papanicolas, Eur. Phys. J. A (2018) **54**: 115.
- [18] C. Alexandrou, J. Berlin, J. Finkenrath, Th. Leontiou and M. Wagner, Phys. Rev. D **101**, 034502 (2020).
- [19] N. G. Antoniou and F. K. Diakonou, J. Phys. G: Nucl. Part. Phys. **46**, 035101 (2019).
- [20] N. G. Antoniou, N. Davis and F. K. Diakonou, Phys. Rev. C **93**, 014908 (2016).

- [21] A. Bialas and R. Peshanski, Nucl. Phys. B **273**, 703 (1986); A. Bialas and R. Peshanski, Nucl. Phys. B **308**, 857 (1988).
- [22] N. G. Antoniou *et al.*, Nucl. Phys. A **693**, 799 (2001)
- [23] N. G. Antoniou *et al.*, Phys. Rev. Lett. **97**, (2006) 032002.
- [24] W. J. Metzger, “*Estimating the Uncertainties of Factorial Moments*”, HEN-455 (2004) (unpublished).
- [25] B. Efron, Ann. Stat. **7**, 1 (1979); T. Hesterberg *et al.*, *Bootstrap Method and Permutation Tests* (W. H. Freeman & Co., USA, 2003), ISBN-10:0716757265.
- [26] R. J. Glauber, Nucl. Phys. A **774** (2006) 3.
- [27] H. de. Vries ADNDT **36** (1987) 495.
- [28] I. Angeli *et al.*, ADNDT **99** (2013) 69.
- [29] C. Alt *et al.* [NA49 Collaboration], Eur. Phys. J. C **45** (2006) 343, and references therein.
- [30] N. Abgrall *et al.* [NA61 Collaboration], JINST **9** (2014) P06005.
- [31] M. Kielbowicz for the NA61/SHINE Collaboration, talk at the XIII Workshop on Particle Correlations and Femtoscopy, Cracow, May 2018 (slides).
- [32] T. Anticic *et al.*, Phys. Rev. C **70**, 034902 (2004).
- [33] M. M. Tsypin, Phys. Rev. Lett. **73**, 2015 (1994).
- [34] N. G. Antoniou, F. K. Diakonov, X. N. Maintas and C. E. Tsagkarakis, in preparation.
- [35] S. Datta, R. V. Gavai and S. Gupta, Phys. Rev. D **95**, 054512 (2017).

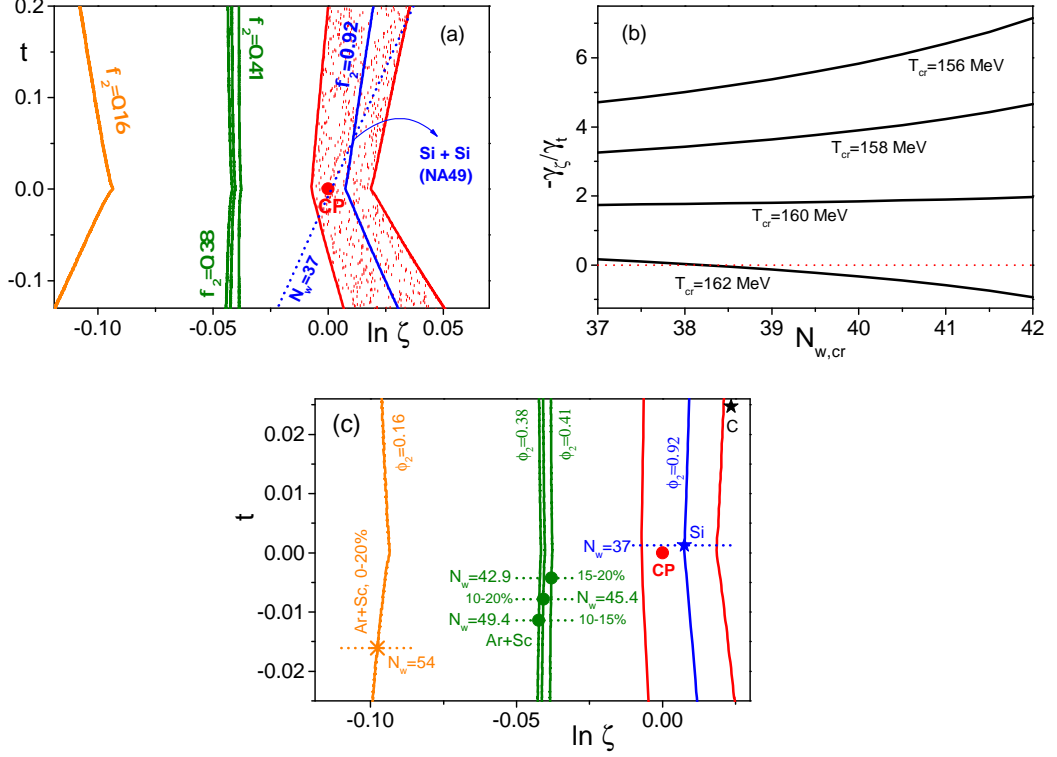


Figure 9: (a) The lines $\phi_2 = \text{constant}$ in the $(\ln \zeta, t)$ plane. The red lines are the borders of the critical region (red shaded area). The blue line corresponds to $\phi_2 = 0.92$ associated with the Si + Si freeze-out state (0 – 12% centrality, 158A GeV/c collision energy) measured in NA49 experiment (SPS,CERN). The three dark green lines correspond to $\phi_2 = 0.41, 0.39$ and 0.38 (from right to left) associated with the Ar + Sc freeze-out states (peripheralities 15 – 20%, 10 – 20% and 10 – 15% respectively) at 150A GeV/c (NA61/SHINE experiment). Finally, the orange line corresponds to $\phi_2 = 0.16$ associated with Ar + Sc freeze-out state in 0 – 20% periphery. The blue dotted line corresponds to $N_w = 37$ line choosing $T_{cr} = 156$ MeV and $N_{w,cr} = 39.5$. The intersection of the two blue lines defines the location of the Si + Si freeze-out state in the $(\ln \zeta, t)$ plane. (b) The slope parameter $-\frac{\gamma_\zeta}{\gamma_t}$ of the $N_w = \text{constant}$ lines versus $N_{w,cr}$ for different values of T_{cr} . (c) The lines $\phi_2 = \text{constant}$ (coloured, solid) and $N_w = \text{constant}$ (coloured, dotted), for the various systems considered, when $\gamma_\zeta = 0$ and $T_{cr} = 162$ MeV. Their intersection defines the associated freeze-out states. The black star represents the C + C freeze-out state (NA49 experiment) in the $(\ln \zeta, t)$ plane.